

Cell wall targeted *in planta* iron accumulation enhances biomass conversion and seed iron concentration in *Arabidopsis* and rice

Haibing Yang^{1,2,3}, Hui Wei⁴, Guojie Ma^{1,2}, Mauricio S. Antunes^{1,3,†}, Stefan Vogt⁵, Joseph Cox^{1,2}, Xiao Zhang², Xiping Liu^{1,2}, Lintao Bu⁶, S. Charlotte Gleber⁵, Nicholas C. Carpita^{3,7}, Lee Makowski^{8,9}, Michael E. Himmel⁴, Melvin P. Tucker⁵, Maureen C. McCann^{1,3}, Angus S. Murphy^{1,2,10,*} and Wendy A. Peer^{1,2,10,11}

¹Center for Direct Catalytic Conversion Of Biomass to Biofuels (C3Bio), Purdue University, West Lafayette, IN, USA

²Department of Horticulture, Purdue University, West Lafayette, IN, USA

³Department of Biological Sciences, Purdue University, West Lafayette, IN, USA

⁴Biosciences Center, National Renewable Energy Laboratory, Golden, CO, USA

⁵X-ray Science Division, Advanced Photon Source, Argonne National Laboratory, Argonne, IL, USA

⁶National Bioenergy Center, National Renewable Energy Laboratory, Golden, CO, USA

⁷Department of Botany and Plant Pathology, Purdue University, West Lafayette, IN, USA

⁸Department of Bioengineering, Northeastern University, Boston, MA, USA

⁹Department of Chemistry and Chemical Biology, Northeastern University, Boston, MA, USA

¹⁰Department of Plant Science and Landscape Architecture, University of Maryland, College Park, MD, USA

¹¹Department of Environmental Science and Technology, University of Maryland, College Park, MD, USA

Received 13 June 2014;

revised 12 February 2016;

accepted 23 February 2016.

*Correspondence (Tel +1-301-405-6244;

fax +1-301-314-9308; email

asmurphy@umd.edu)

†Present address: Department of Biology, Colorado State University, Fort Collins, CO 80523, USA.

Keywords: biofuel, cell wall, secretion, iron-binding peptide, carbohydrate-binding module, iron concentration.

Summary

Conversion of nongrain biomass into liquid fuel is a sustainable approach to energy demands as global population increases. Previously, we showed that iron can act as a catalyst to enhance the degradation of lignocellulosic biomass for biofuel production. However, direct addition of iron catalysts to biomass pretreatment is diffusion-limited, would increase the cost and complexity of biorefinery unit operations and may have deleterious environmental impacts. Here, we show a new strategy for *in planta* accumulation of iron throughout the volume of the cell wall where iron acts as a catalyst in the deconstruction of lignocellulosic biomass. We engineered CBM-IBP fusion polypeptides composed of a carbohydrate-binding module family 11 (CBM11) and an iron-binding peptide (IBP) for secretion into *Arabidopsis* and rice cell walls. CBM-IBP transformed *Arabidopsis* and rice plants show significant increases in iron accumulation and biomass conversion compared to respective controls. Further, CBM-IBP rice shows a 35% increase in seed iron concentration and a 40% increase in seed yield in greenhouse experiments. CBM-IBP rice potentially could be used to address iron deficiency, the most common and widespread nutritional disorder according to the World Health Organization.

Introduction

As the world population continues to increase and fossil resources are finite, alternative feedstocks for fuels and other chemicals are being developed to meet this growing demand (Hill *et al.*, 2006). Nongrain lignocellulosic biomass feedstocks, such as rice straw, are sustainable resources because they are renewable, abundant and are not used as human food (Himmel *et al.*, 2007). In addition to fuel, low-cost lignocellulosic biomass can be converted into high-value products in selective biorefinery processes. Unfortunately, thermal and chemical conversions require high-energy inputs and the efficiency of biochemical conversion is limited by biomass recalcitrance. A strategy to reduce initial energy inputs and facilitate the deconstruction of cell walls (Wei *et al.*, 2011) involves use of transition metal catalysts, such as

Fe^{2+} . However, pretreatments in which the metal catalysts are directly added to biomass will increase unit operations and costs, and the high concentrations of metal required to penetrate the cell walls present potential environmental problems of water usage and disposal.

Furthermore, a method that increases iron accumulation in rice grain is important to combat iron deficiency in human populations which rely on this low-iron grain for subsistence (Meng *et al.*, 2005; Goto *et al.*, 1999). Transition metal uptake, transport and homeostatic mechanisms are tightly coordinated, and efforts to engineer iron-enriched crops for food and metal hyperaccumulating plants for phytoremediation have achieved limited success after 25 years of research (Palmer and Guerinot, 2009). Translation of Ni^{2+} hyperaccumulation mechanisms to Fe^{2+} , Cu^{2+} and Mn^{2+} accumulation is limited as cytosolic Fe^{2+} ,

Please cite this article as: Yang, H., Wei, H., Ma, G., Antunes, M.S., Vogt, S., Cox, J., Zhang, X., Liu, X., Bu, L., Gleber, S.C., Carpita, N.C., Makowski, L., Himmel, M.E., Tucker M.P., McCann M.C., Murphy, A.S. and Peer, W.A. (2016) Cell wall targeted *in planta* iron accumulation enhances biomass conversion and seed iron concentration in *Arabidopsis* and rice. *Plant Biotechnol. J.*, doi: 10.1111/pbi.12557

Cu^{2+} and Mn^{2+} levels required for effective cell wall catalysis are toxic to living plants. Therefore, the challenge is to avoid cellular toxicity and, at the same time, accumulate transition metals throughout the volume of the cell wall, both to reduce biomass recalcitrance in vegetative tissues and to increase iron concentration in grain. Here, a combination of strategies was used to tailor plants for increased transition metal concentration to facilitate direct catalysis of cell wall deconstruction. An unexpected consequence of this approach was enhancement of iron in rice grains.

Results and discussion

Design and synthesis of CBM-IBP constructs

Figure 1a shows the approach used to increase transition metal concentration *in planta* for efficient cell wall deconstruction by fusing an iron-binding peptide (IBP), a carbohydrate-binding module (CBM) to bring the IBP near carbohydrate bonds in the cell wall and a signal peptide (SP) so that the SP-CBM-IBP

polypeptide would be secreted to the cell wall. Several constitutive and inducible constructs were designed that contained the SP-CBM-IBP polypeptide and different tags, for example haemagglutinin (HA) or a fluorescent protein (Figure 1a and Figure S1a). Two iron-binding peptides (IBP) were synthesized and analysed for metal binding: a minimal ferritin-binding peptide based on the ferritin monomer and a synthetic blood iron-binding motif based on the blood iron-binding peptide that we had previously isolated and found that it bound iron across a wide range of pH. Both the synthetic blood IBP DLGEQYFKG (Lee and Song, 2009) and the ferritin IBP LAEEKREGYER (Lawson *et al.*, 1991) bound iron *in vitro* at cytosolic pH ~7.0 and apoplastic pH ~5.5 (Figure 1b,c). An extensin secretion signal peptide (SP) (De Loose *et al.*, 1991) was chosen for secretion of the SP-CBM-IBP polypeptide into the cell wall. Signal peptides have been used to successfully secrete carbohydrate-binding modules (CBMs) in poplar, Arabidopsis and rice (Cho and Cosgrove, 2000; Choi *et al.*, 2003).

Clostridium thermocellum CBMs were used to target the IBPs to carbohydrate components of the cell wall. The pool of CBMs

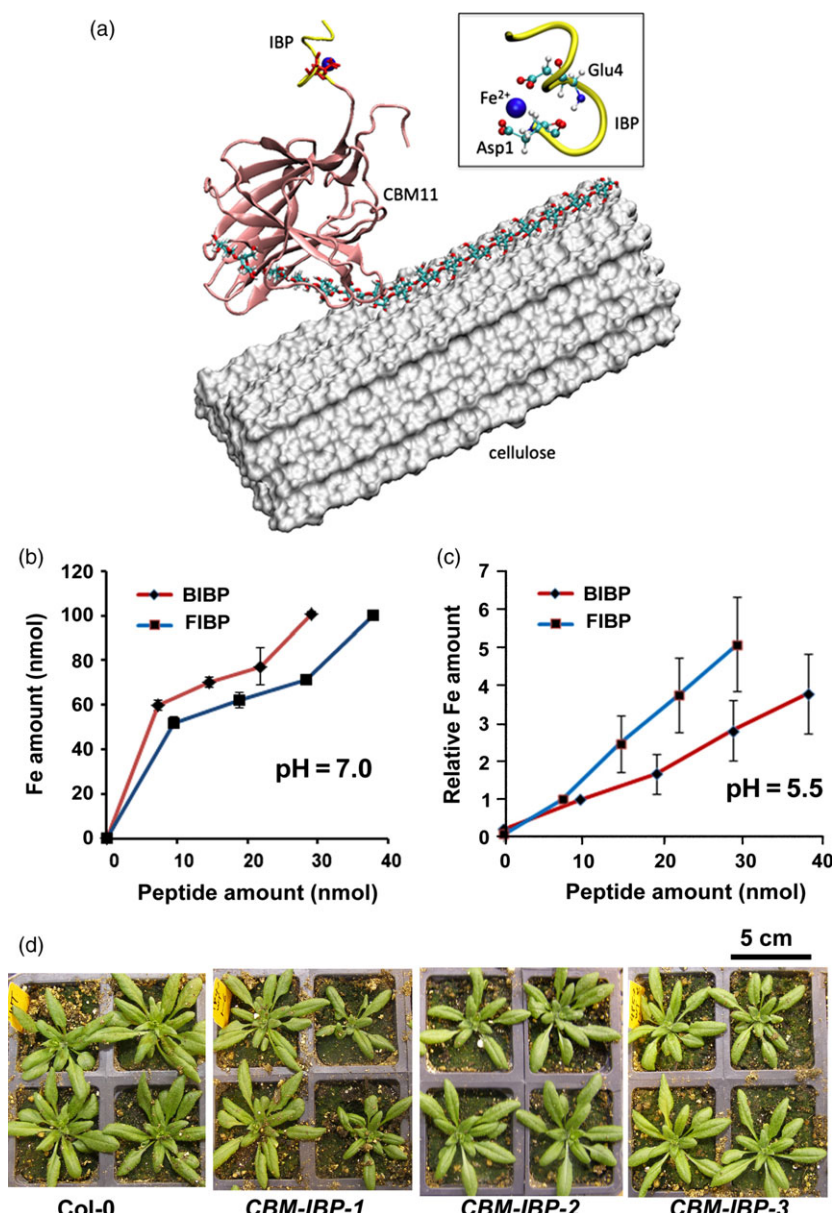


Figure 1 Design and generation of CBM-IBP constructs and Arabidopsis plants. (a) Putative model of CBM11-IBP (*CtCBM11*: pink, synthetic blood IBP: yellow) binding to the cell wall. The CBM11-IBP is placed on the hydrophobic surface of a microfibril, represented as white surface. An edge chain was pulled up from the cellulose surface and bound in the binding cleft of *CtCBM11*. Inset: The Fe^{2+} -binding site in IBP is highlighted (red: oxygen atoms; Fe^{2+} : blue sphere). (b, c) Iron-binding assays of the synthetic blood iron-binding peptide (BIBP) and ferritin iron-binding peptide (FIBP) at pH 7.0 and pH 5.5. Values are mean \pm standard deviation (SD), $n = 3$ technical replicates. (d) Representative images of 28-days Col-0 and three independent homozygous CBM-IBP Arabidopsis transgenic lines; their growth was comparable to Col-0.

is diverse, with each CBM targeting different polysaccharides in the cell wall (Boraston *et al.*, 2004; Shoseyov *et al.*, 2006). Five CBMs with an SP N-terminal fusion and a C-terminal pH-insensitive fluorescent protein mCherry (Shaner *et al.*, 2005) were expressed in *Arabidopsis* under control of a constitutive promoter (SP-CBM-mCherry) and analysed for secretion (Figure S1b). Of the five, three showed intracellular fluorescent signals, and CBM11, which binds primarily 1,4- β and 1,3-1,4- β mixed linked glucans, and CBM22, which binds primarily 1,3- β and 1,4- β glucans (Hashimoto, 2006), showed signals localized to the cell wall, indicating that these two CBMs were successfully secreted, although some intracellular signal was observed (Figure S1b). Higher fluorescent signals were observed in the *SP-CBM11-mCherry* plants compared to *SP-CBM22-mCherry* plants (Figure S1b); therefore, CBM11 was used for further analyses. IBPs were then fused to the secreted CBM11 (*SP-CBM11-IBP*) to target the iron to carbohydrate bonds in the cell wall as shown in Figure 1a. Modelling of *SP-CBM11-IBP* docking to cellulose microfibrils suggests that iron targeting to cell walls is possible (Wu *et al.*, 2013), although this remains to be demonstrated *in planta*. CBM11 fused to the minimal ferritin iron-binding peptide (*SP-CBM11-FIBP*) did not show obvious signals in the cell wall in *Arabidopsis thaliana* (data not shown) and was not analysed further. Secreted CBM11 fused to the synthetic blood iron-binding peptide and HA (*SP-CBM11-IBP-HA*), hereafter called CBM-IBP, showed a range of relative expression levels (Figure S1c). Whereas metal hyperaccumulating plants often show reduced growth (Palmer and Guerinot, 2009), a wide range of *CBM-IBP* expression levels had no detrimental effect on plant growth when expressed in *Arabidopsis thaliana* (Figure 1d and Figure S1d).

CBM-IBP localizes to cell walls in *Arabidopsis*

To determine whether CBM-IBP was secreted to the cell wall, CBM-IBP localization was analysed under the control of a tamoxifen-inducible promoter (*CBM-IBP-Dendra2*) or a constitutive promoter (*CBM-IBP-HA*). No autofluorescence in roots and only chlorophyll autofluorescence in hypocotyls and cotyledons were observed in uninduced plants (Figure 2a,d,g). After induction, CBM-IBP-Dendra2 signals were observed in roots (Figure 2b,c), cotyledons (Figure 2e,f) and hypocotyls (Figure 2h), and apoplastic localization was observed following plasmolysis (Figure 2c,f,h). Upon induction, the intracellular localization was most pronounced in younger tissue, that is cells close to the root tip (Figure 2c), compared to mature tissue, consistent with the greater activity of the secretory system in actively growing cells (De Loose *et al.*, 1991; Hall and Cannon, 2002; Lamport *et al.*, 2011); unsecreted CBM-IBP may bind to the cell wall during senescence. Immunohistochemistry of constitutively expressed CBM-IBP-HA also showed apoplastic localization (Figure 2j,l), and no signal was detected in plants transformed with the empty vector (Figure 2i,k). Further, X-ray fluorescence microscopy, in which each pixel is analysed for elemental fluorescence, showed that iron signals were localized to the cell walls of the epidermis as well as the vascular tissue in mature stems (Figure 2m,n); calcium (Figure 2m,n) and zinc (not shown) signals were observed in the cell walls throughout the stem. Iron quantification using an absolute scale could not be obtained due to variations in section thickness. These data suggest that CBM-IBP could bind the iron at the cell wall and suggested the possibility of iron deposition in the cell wall may have occurred via the secretory pathway. Whereas both

inducible and constitutive expression resulted in CBM-IBP accumulation at the cell wall, plants with constitutively expressed HA fusion polypeptides were chosen for further analyses due to tamoxifen toxicity.

CBM-IBP* enhances iron concentration in *Arabidopsis

Arabidopsis thaliana plants expressing *CBM-IBP* showed increased iron concentration in shoots and seeds and enhanced biomass conversion in shoots (Figure 3). *CBM-IBP* shoots contained 60%–70% more iron compared to wild-type control plants ($P < 0.05$, Figure 3a). Perls' Prussian blue staining was used to visualize iron accumulation directly *in planta*. *CBM-IBP* *Arabidopsis* leaves showed more staining than controls, indicating increased iron accumulation (Figure 3b). To determine whether the iron-binding peptide was responsible for the increased iron concentration, the DLGEQYFKG residues in CBM-IBP were mutated to VLGVIVYIVG (*CBM-IBP Δ*) which abolishes the iron-binding motif E/DXXE (Fang and Wang, 2002; Lawson *et al.*, 1991). *CBM-IBP Δ* *Arabidopsis* lines with a range of expression levels comparable to the *CBM-IBP* lines were analysed (Figure S2a and Figure S1c). *CBM-IBP Δ* plants had iron concentrations comparable to wild type (Figure 3a and Figure S2b); therefore, the CBM-IBP, but not CBM-IBP Δ , binds iron and increases iron amounts *in planta*.

The iron accumulation in seeds was analysed to assess whether CBM-IBP could also enhance iron accumulation in other tissues. Iron is naturally high in *Arabidopsis* seeds, and *CBM-IBP-2* seeds showed increased iron accumulation compared to wild type ($P = 0.002$), and *CBM-IBP-1* and *CBM-IBP-3* were similar to wild type ($P = 0.09$, $P = 0.11$, respectively; Figure 3c). However, significantly more iron accumulated in seeds when *CBM-IBP* was expressed in the *oligopeptide transporter 3-2* (*opt3-2*) mutant background ($P < 0.01$, Figure 3c) which has reduced iron concentration in seeds (Stacey *et al.*, 2008). These results indicate that CBM-IBP-mediated iron increases are distinct from OPT3-dependent iron accumulation in *Arabidopsis* seeds (Stacey *et al.*, 2008), and indicate that CBM-IBP can increase iron accumulation in plants that have low amounts of iron.

CBM-IBP* enhances biomass conversion in *Arabidopsis

Previously, we developed a dilute acid/Fe²⁺ pretreatment for biomass that increased the yield of sugar monomers (Wei *et al.*, 2011). Moreover, the hot water/Fe²⁺ and hot water/Fe³⁺ pretreatments were also effective in releasing more simple sugars than hot water alone pretreatment (Kamireddy *et al.*, 2013; Liu *et al.*, 2009; Zhao *et al.*, 2011). *Arabidopsis* plants expressing *CBM-IBP* or *CBM-IBP Δ* were analysed using this process, that is without adding exogenous Fe²⁺. *CBM-IBP* shoots yielded 20% more glucose and 15% more xylose compared to controls ($P < 0.05$, Figure 3d and Figure S2c). The enhanced release of sugar monomers can be attributed to iron binding by IBP, as *CBM-IBP Δ* shoots showed glucose and xylose release comparable to wild type ($P > 0.05$, Figure 3d and Figure S2c). Total cellulose and ethanol-soluble and ethanol-insoluble sugars in *CBM-IBP* biomass were not different from wild type and *CBM-IBP Δ* controls ($P > 0.05$, Figure S2d–f). Therefore, a functional iron-binding motif in CBM-IBP is necessary to enhance cell wall hydrolysis in *CBM-IBP* plants. This is also consistent with iron reduction in biomass recalcitrance under acidic conditions in pretreatments (Wei *et al.*, 2011) and demonstrates that iron accumulated *in planta* appears to function in the same manner.

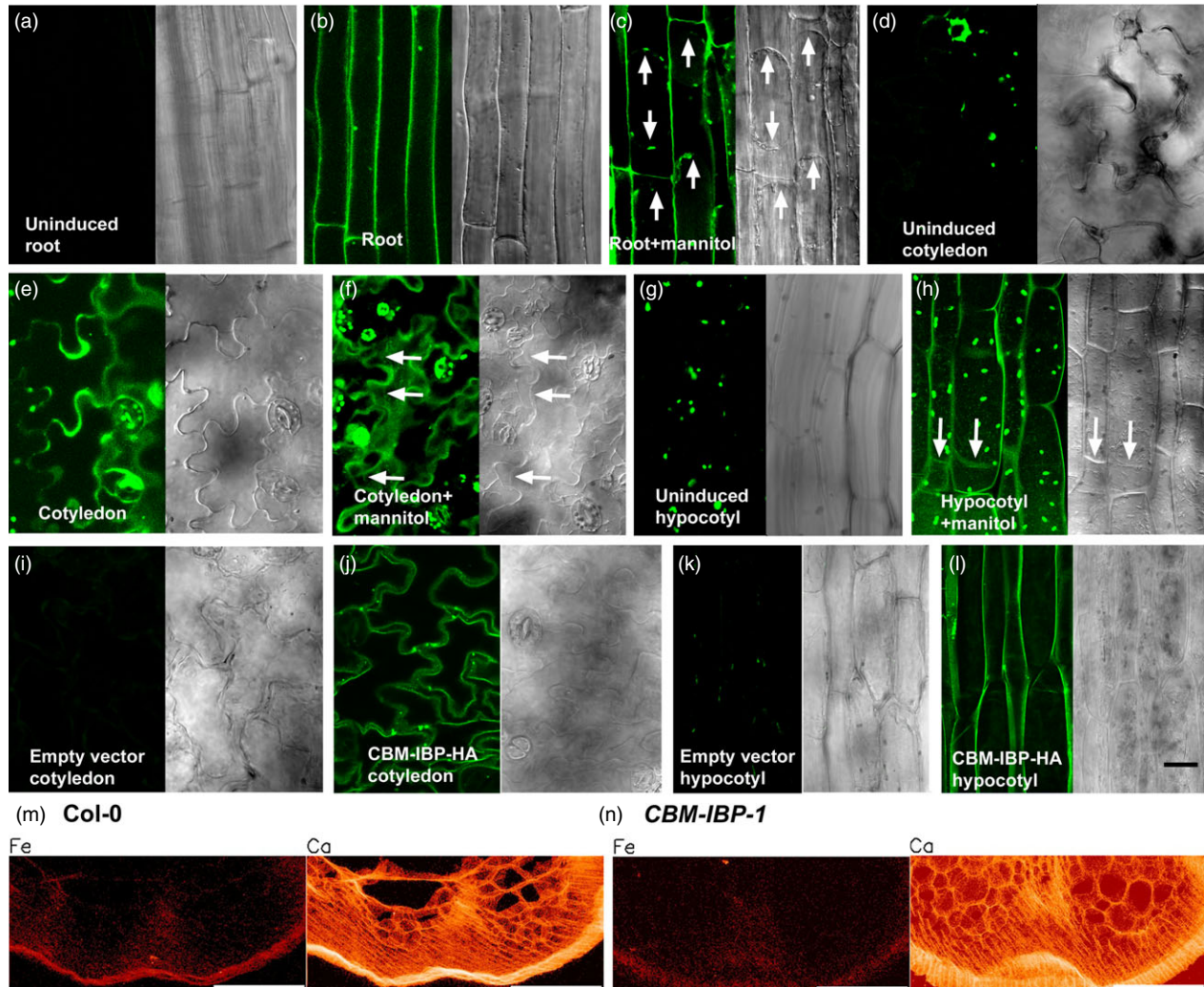


Figure 2 CBM-IBP and iron ions localize to cell walls in Arabidopsis. (a–h) Expression and localization of the oestrogen-inducible CBM-IBP-Dendra2 fluorescent protein in Arabidopsis without (a, d, g) and with (b, c, e, f, h) 4 µM 4-hydroxytamoxifen for 16–40 h. (c, f, h) Cell wall and intracellular signals were observed after plasmolysis with 0.6 M mannitol. Arrows indicate the position of the plasma membrane following plasmolysis. (i–l) Immunohistochemistry of CBM-IBP-HA in Arabidopsis with anti-HA showed cell wall and intracellular localization in hypocotyls and cotyledons; controls transformed with empty vector plasmid showed no signal. Scale bar = 20 µm. (m, n) Iron localization analysed by X-ray fluorescence microscopy showed cell wall localization of Fe in inflorescence stem sections of 4-week-old Col-0 and *CBM-IBP-1* plants (see methods). Ca²⁺ localization is shown as a reference to indicate cell walls. Scale bar = 100 µm.

CBM-IBP enhances iron concentration and biomass conversion in rice

There is some question whether the success of iron accumulation in increasing monomer sugar release in Arabidopsis would transfer to grasses. Arabidopsis cell walls are typical of dicotyledonous species, but the cell walls of grass species such as rice contain additional noncellulosic polysaccharides. Further, Arabidopsis uses a reduction strategy for iron uptake, while rice uses a combination of reduction and chelation (Palmer and Guerinot, 2009). Wild-type rice was transformed with *CBM-IBP* to test whether the same *in planta* technology can be translated to crop rice. Homozygous transgenic rice lines that expressed *CBM-IBP* were selected for analyses (Figure 4a and Figure S3a). *CBM-IBP* rice shoots had ~60% increase in iron accumulation compared to wild type ($P < 0.05$, Figure 4b), similar to the increase observed in *CBM-IBP* Arabidopsis. Perls' Prussian blue staining also showed

increased iron levels in *CBM-IBP* rice roots and leaves (Figure 4c), with staining most pronounced in xylem cells (Figure 4d). Without exogenous Fe²⁺ in the pretreatment, release of glucose and xylose from *CBM-IBP-2* rice shoots was comparable to *CBM-IBP* Arabidopsis plants, yielding 25% more glucose and 15% more xylose compared to controls ($P < 0.05$, Figure 4e). Total cellulose, ethanol-soluble and ethanol-insoluble sugars in *CBM-IBP* rice biomass were similar to wild type ($P > 0.05$, Figure S3b,c,d). Further, the amount of glucose released was greater in the 2M trifluoroacetic acid (TFA)-soluble fraction and reduced in the nonsoluble pellet ($P < 0.05$, Figure 3c). As rice and Arabidopsis have similar cellulose structures and differential effects of CBM11 expression in rice and Arabidopsis are unlikely, CBM-IBPA analyses were not repeated in rice. These results demonstrate that iron accumulated *in planta* efficiently facilitates biomass deconstruction, although the effects of iron on the synthesis of other polymers to enhance saccharification cannot be ruled out.

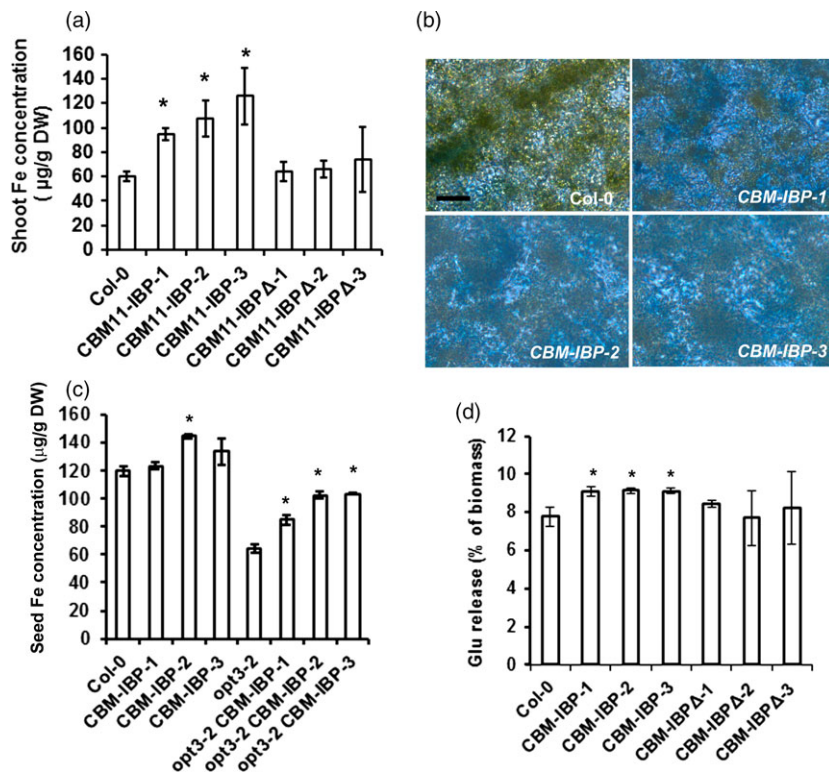


Figure 3 *CBM-IBP* enhances iron concentration and biomass conversion in *Arabidopsis*. (a) Shoot iron concentration was greater in *CBM-IBP* *Arabidopsis* lines compared to Col-0 and *CBM-IBPΔ* harbouring mutations in iron-binding sites. (b) Perls' staining showed more iron concentration (blue) in *CBM-IBP* *Arabidopsis* leaves than Col-0 leaves. Scale bar = 50 µm. (c) Iron concentration in seeds was increased by expression of *CBM-IBP* in *Arabidopsis* mutant *opt3-2*, *oligopeptide transporter 3-2*, and *Arabidopsis* mutant has less iron in seeds than wild type. Values are mean ± SD, n = 3 biological replicates. *, P < 0.05, Student's t-test, compared to corresponding control. (d) Glucose (Glu) yield from *CBM-IBP* *Arabidopsis* dry shoots was greater than Col-0 and *CBM-IBPΔ*. Values are mean ± SD, n = 3 biological replicates. *, P < 0.05, by Student's t-test compared to corresponding control.

CBM-IBP increases yield and iron concentration in rice seeds

As iron hyperaccumulation may reduce growth and/or yield, the growth of *CBM-IBP* rice plants was analysed in detail. Rice expressing *CBM-IBP* senesced slightly earlier than wild type based on the colour and chlorophyll levels of older flag leaves when the panicles were fully filled (Figure 4a; Figure S3f). The *CBM-IBP* rice homozygous lines had reduced height compared to wild type (Figure 4a and Figure S3e). Whereas short stature is a favourable trait for grain production in rice, it is not for biomass production. However, *CBM-IBP* rice plants developed more tillers (P < 0.05, Figure 5a), and, offsetting their short statures, the shoot dry weight of *CBM-IBP-1* and *CBM-IBP-2* rice was greater than wild type (P < 0.05, Figure 5b). Plants in the greenhouse were grown at the same density as in the field, and tillering of wild-type rice in the greenhouse was comparable to field-grown rice. *CBM-IBP* rice plants also produced ~40% more seeds per plant compared to wild type (P < 0.05, Figure 5c), which will be re-evaluated in field trials. Chlorophyll quantifications were greater in *CBM-IBP* mature green flag leaves and less in yellow flag leaves compared to wild type (P < 0.05, Figure S3f). The increased chlorophyll concentration in the *CBM-IBP* flag leaves is consistent with increased seed yield and iron concentrations in biomass and seeds (described below). Rice tillering is modulated by strigolactones, and DWARF 27 (D27), an iron-binding isomerase that converts *trans*-β-carotene into 9-*cis*-β-carotene in the strigolactone biosynthetic

pathway (Alder *et al.*, 2012; Lin *et al.*, 2009). Increased iron may affect D27 activity and/or function and subsequently influence tillering activity, although how iron may affect D27 or other factors regulating tillering is unknown. Furthermore, iron promotes chlorophyll biosynthesis (Chereskin and Castelfranco *et al.*, 1982) which may have increased the biomass yield in transgenic plants; however, such hypotheses need to be tested in future experiments.

The iron accumulation in *CBM-IBP* dehusked brown rice seeds (brown rice, also known as unmilled or unpolished rice) was analysed to determine whether an iron increase similar to *CBM-IBP* *Arabidopsis* occurred. *CBM-IBP* rice seeds had 35% (*CBM-IBP-1*) to 37% (*CBM-IBP-3*) more iron than wild-type seeds (P < 0.05, Figure 5d; Table S1). *CBM-IBP* rice contained 17–23 µg iron/g dry weight, which is comparable to iron accumulation in rice overexpressing soya bean ferritin (12–20 µg iron/g dry weight, Qu *et al.*, 2005) or hydroponically grown *NFP* brown rice overexpressing two transgenes, nicotianamine and ferritin in the endosperm (17 µg iron/g dry weight, Wirth *et al.*, 2009). Iron levels in milled rice (white rice or polished rice) increased ~two-fold in *CBM-IBP-1* and ~three-fold in *CBM-IBP-2* and *CBM-IBP-3* compared to wild type (P < 0.05, Figure 5e). The iron increase in *CBM-IBP* white rice (4–6 µg iron/g dry weight) was comparable to *NFP* white rice (~7 µg iron/g dry weight). The average seed weight and size (length, width, area) were similar among *CBM-IBP* and wild-type rice grains (P > 0.1, Figure S4a–e), and therefore, the average iron amount per grain was greater in

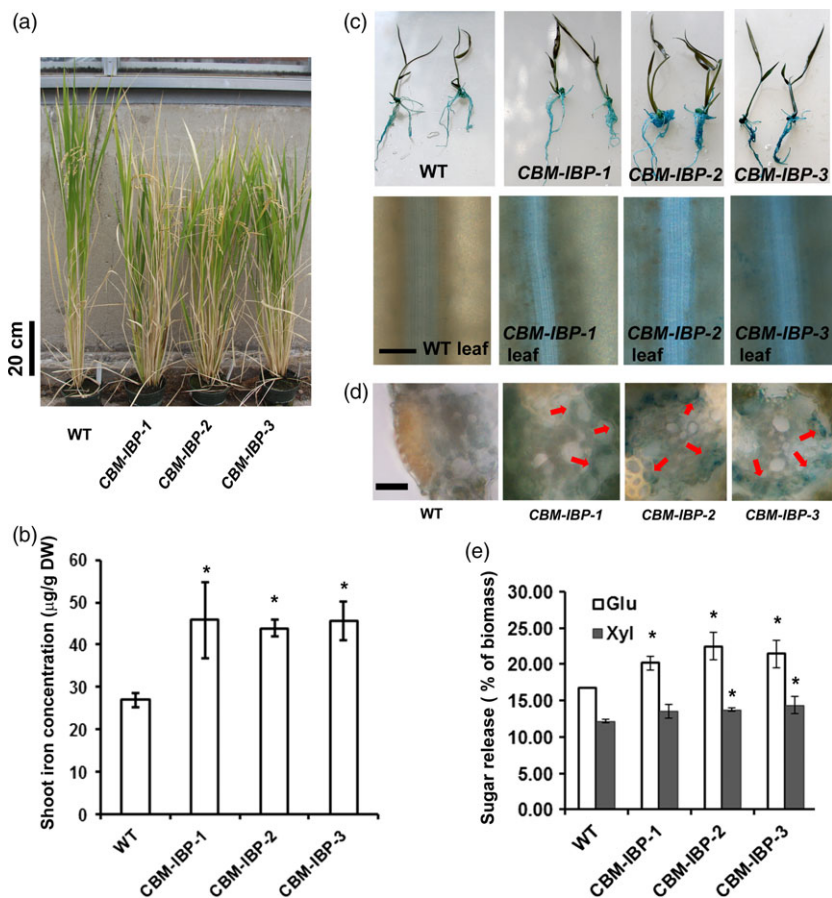


Figure 4 CBM-IBP enhances iron concentration and biomass conversion in rice. (a) Representative image of 120-d-old wild-type (WT) and independent homozygous CBM-IBP transgenic lines. (b) Shoot iron concentration was greater in CBM-IBP rice lines than WT. (c) Perls' staining showed greater iron concentration in CBM-IBP rice leaves than WT leaves. Scale bar = 100 μ m. (d) Perl's staining on cross sections shows iron localization in vascular tissue. Scale bar = 20 μ m. (e) Glucose and xylose yields from CBM-IBP rice straw were greater than that from WT. Values are mean \pm SD, $n = 3$ biological replicates. *, $P < 0.05$, by Student's *t*-test compared to corresponding control.

CBM-IBP than wild type. Furthermore, peptide-chelated iron may be more bioavailable for absorption (Lee and Song, 2009). Analysis of the ion profile in both *Arabidopsis* and rice seeds indicated some increases in other metal ions for which there are toxicity concerns, such as Cd, Co, Cr and Cu (Table S1). However, the concentration of the metal ions measured was below the toxic limits set by FDA (www.fda.gov) based on consumption of 1 kg dry brown rice per day. For reference, the average consumption is ~0.5–0.6 kg rice per day by individuals in the highest rice-consuming countries. If implemented in the field, cultivar selection for biofuels and/or biofortification characteristics should be considered because of genetic variation in mineral concentration among rice cultivars (2–45 μ g iron/g dry weight brown rice, Zheng *et al.*, 2010).

Here, a triple fusion polypeptide was used successfully to accumulate iron in the cell wall while avoiding cellular toxicity: (i) the signal peptide from a native cell wall extension protein to provide efficient secretion (De Loose *et al.*, 1991), (ii) a synthetic blood iron-binding peptide to efficiently bind iron and (iii) CBM11 to direct the IBP-bound iron to cell wall polysaccharides to prevent re-uptake of free iron into the cell (Palmer and Guerinot, 2009) resulting in enhanced biomass conversion. In contrast to the millimolar iron added to feedstock postharvest (Wei *et al.*, 2011), CBM-IBP plants contain micromolar iron that efficiently and

effectively increases saccharification yield. These results indicate that *in planta* iron targeting to the cell wall can effectively increase saccharification yields in biochemical conversion processes. The release of simple sugars in CBM-IBP rice was at least comparable to the pretreatment of corn stover in Wei *et al.* (2011), suggesting that the plant engineering approach is more efficient than the conventional iron loading approach. The current cultural practices of growing rice, which includes foliar iron applications, would not need to be altered to realize increased iron concentration in CBM-IBP rice. Further, it appears that CBM-IBP rice more efficiently utilizes the iron in the foliar spray than wild type based on the increased amounts of chlorophyll and iron in leaves. It is important to note that biomass recalcitrance varies among different plant tissues, for example leaves versus stems and apical versus basal stems. Some of the observed differences in pretreatment and enzymatic digestibility could be attributed to differences in CBM-IBP plant growth compared to the controls (i.e. shorter stature, thicker stems, more tillers).

It would be unrealistic to consider that straw from CBM-IBP rice would be the only part of the plant used, especially with the need to feed a growing global population. An unintended consequence of expressing CBM-IBP was a ~40% increase in seed yield and 35% increase in seed iron accumulation. Given that a 3%

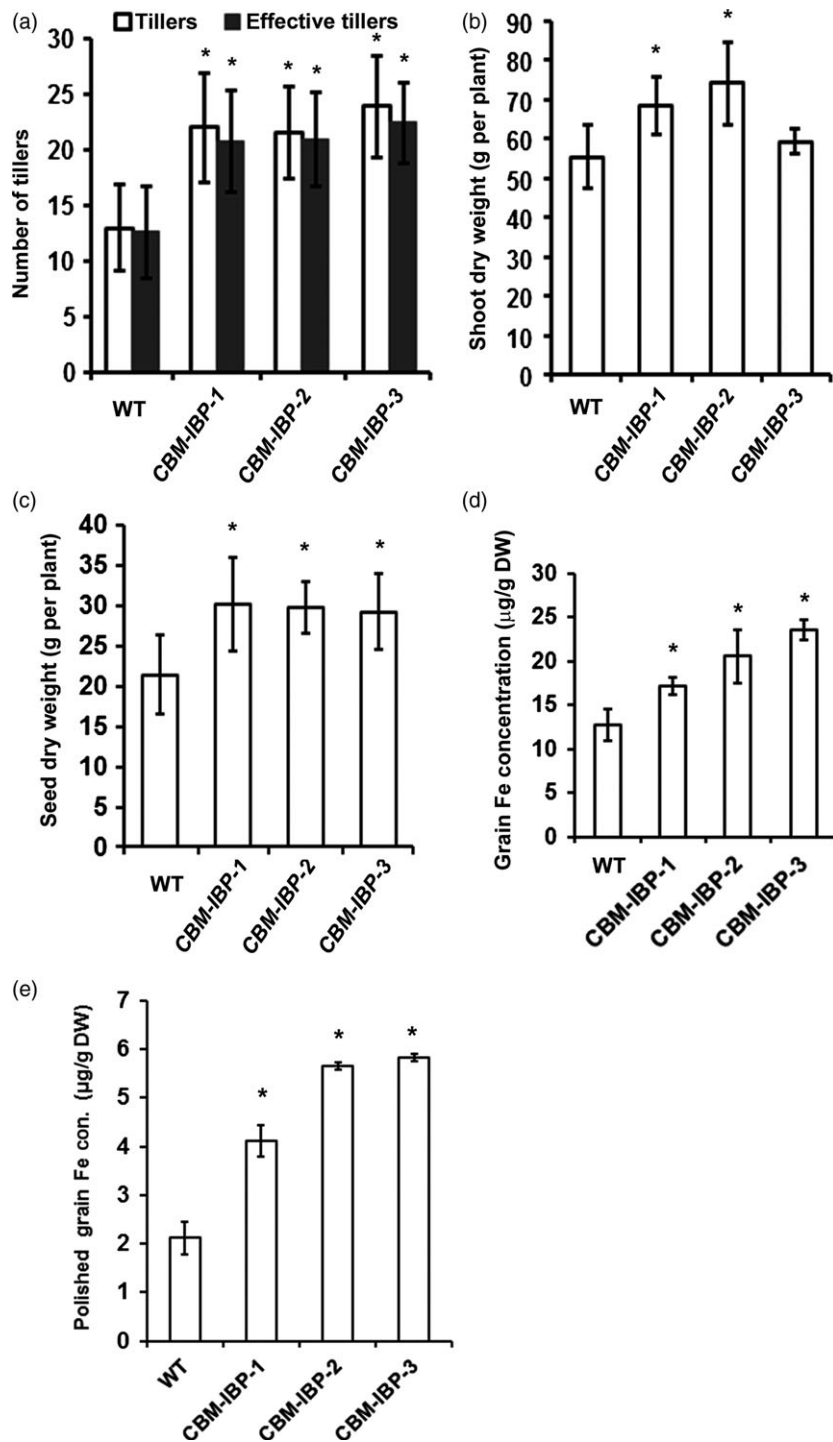


Figure 5 CBM-IBP rice plants showed increased yield and grain iron concentration. (a-c) Number of tillers (effective tillers, tillers producing seeds), shoot dry weight and seed dry weight were greater in homozygous CBM-IBP rice transgenic lines compared to wild type (WT). Values are mean \pm SD, $n = 8$ biological replicates. (d, e) Iron concentration was greater in CBM-IBP dehusked brown rice and polished white grains than controls. Values are mean \pm SD, $n = 3$ biological replicates. *, $P < 0.05$, Student's *t*-test, compared to corresponding control.

increase in yield is considered significant (Baldwin *et al.*, 2012), we will determine whether the enhanced traits are observed under field conditions. The increased iron accumulation in brown and white rice could address iron deficiency, with an apparently low potential for toxicity from other metals. Allergens from the peptides would also be of concern. The IBP has no predicted

antigenic determinants, and CBM11 has five; for comparison, rice α -expansin (CBMs are homologous to expansins) has seven (<http://imed.med.ucm.es>). Taken together, this technology could be used for both enhanced conversion of rice straw biomass to biofuel and increased iron-enriched grain yield to support both global energy and food demands.

Experimental procedures

Constructing the binding model of CtCBM11-IBP to cell wall

The atomistic model of the *CtCBM11* (*Clostridium thermocellum* CBM11) was constructed using the reported NMR structure 2LR0 (Viegas *et al.*, 2013). The blood iron-binding peptide was initially generated as a α -helix and attached to the C-terminal end of *CtCBM11*. The parameters of the Fe^{2+} -binding site in ferritin monomer (Lawson *et al.*, 1991), for example the distances between Fe^{2+} and oxygen atoms, were used to restrain the binding site in the blood Fe-binding peptide. An energy minimization of *CtCBM11*-IBP system was then conducted for 2000 steps of steepest decent minimization followed by 2000 steps adopted basis Newton–Raphson (ABNR) minimization using CHARMM (Brooks *et al.*, 2009). A previously equilibrated cellulose I β microfibril (Beckham *et al.*, 2012; Payne *et al.*, 2011; Wu *et al.*, 2013) was used to construct the *CtCBM11*-IBP/cellulose complex. The microfibril was composed of four layers, which consist of 3, 4, 5 and 6 cellulose chains from the top layer to the bottom layer, respectively. Each cellulose chain has 16 glucose residues. As *CtCBM11* is characterized as a type B subfamily of CBMs and binds to a single cellobextrin chain, the *CtCBM11* was placed on the hydrophobic surface with a single 'edge' cellobextrin chain bound to its binding cleft. The CHARMM22 force field parameters (Brooks *et al.*, 2009; MacKerell *et al.*, 1998) were used for the peptide and the C35 carbohydrate force field parameters (Guvench *et al.*, 2008, 2009) were used for the cellulose during energy minimization. Fe^{2+} and two oxygen atoms at the Fe^{2+} -binding site were harmonically restrained. A final minimization of the entire system was run for 1000 steps of steepest decent minimization followed by 1000 steps ABNR minimization.

Iron-binding peptides and assays

The peptides DLGEQYFKG (ferritin iron-binding peptide, FIBP, molecular weight 1057) and LAEEKREGYER (blood iron-binding peptide, BIBP, MW 1380) were synthesized by Cambridge Research Biochemicals (www.crbdiscovery.com). For IBP-binding assay at pH 7.0 phosphate buffer, free Fe^{2+} forms insoluble compound with phosphate and removed by centrifugation. IBP-bound Fe in the supernatant was determined by orthophenanthroline which results a red solution when binds with Fe^{2+} . The iron-binding assay at pH 7.0 was performed in 500 μL binding solution [20 mM MES pH 7.0; 0.5 mM FeCl_2 ; peptide (2 mg/mL, 50 mM phosphate buffer pH 7.0): 0, 5, 10, 15, and 20 μL ; H_2O up to 500 μL , 2 mM final phosphate] at room temperature for 1 h with gentle shaking according to Lee and Song (2009). The binding solution was spun at 3500 $\times g$ for 30 min to remove precipitates. The iron concentration in the supernatant was determined using a colorimetric method (adapted from Harris, 1998) by orthophenanthroline which results in a red solution when binds with Fe^{2+} . Hydroquinone is added to prevent oxidation of Fe^{2+} to Fe^{3+} . One hundred μL supernatant was transferred to a new microcentrifuge tube to which 20 μL 1% hydroquinone and 50 μL 0.25% orthophenanthroline and 830 μL H_2O were added to make the final volume 1 mL, and the absorbance at 510 nm was determined. The iron-binding assay at pH 5.5 was performed as above with the following modifications due to the solubility of the iron at pH 5.5: 100 μL binding solution (20 mM MES pH 5.5; 2.5 mM FeCl_2) was used for

the assays and 20 μL supernatant was blotted onto polyvinylidene difluoride (PVDF) membrane. The membranes were washed with 20 mM MES pH 5.5 buffer twice for 5 min each time. The membranes were developed in 5 mL developing solution (100 μL 1% hydroquinone, 250 μL 0.25% orthophenanthroline) and imaged, and the colour intensity was analysed with ImageJ software (rsbweb.nih.gov/ij/).

Constructs

All primers used in this work are listed in Table S2. The extensin signal peptide (SP) and the carbohydrate-binding module (CBM) cassettes *SP-CBMs-mCherry* and *SP-CBM11-Roo* were constructed using overlapping PCR primers. After digestion with BamHI and SacI, the *SP-CBMs-mCherry* and *SP-CBM11-Roo* cassettes were cloned into *pCAMBIA2300* (www.cambia.org/daisy/cambia/585). The *SP-CBM11-IBP* (blood iron-binding peptide) cassette called *CBM-IBP* was amplified from *pCambia2300-SP-CBM11-Roo* using the primers CaccSP-5' and BIBP-3' and cloned into Gateway entry vector *pENTR/TOPO* (Invitrogen, www.invitrogen.com). The *CBM-IBPΔ* cassette containing the mutated blood iron-binding motif (*BIBPΔ*) was amplified from *pENTR-CBM-IBP* using the primers CaccSP-5' and BIBPΔ-3' and cloned into *pENTR/TOPO*. The constructs were analysed by PCR and restriction digests, and were sequenced using the M13 forward primer. The plasmids *pENTR-CBM11-IBP/BIBPΔ* were cut with *Mlu*I, and the *CBM11-IBP/BIBPΔ* cassettes were transferred to *pGWB14* (Nakagawa *et al.*, 2007) (with C-terminal HA fusion) and/or the oestrogen-inducible vector *pIST04* (modified from *pEarleyGate101* with N-terminal oestrogen-inducible elements: FMV:NEV + 10x NIP promoter and C-terminal Dendra2 fusion) (Jásik *et al.*, 2013) using LR reactions (Invitrogen).

Plant transformation

Arabidopsis was transformed with the constructs by the floral dip method (Clough and Bent, 1998). The resulting transformants were selected on 0.45% phytigel plates containing quarter-strength Murashige and Skoog (MS) basal salts, pH 5.5, at 22 °C, 14 h 100 $\mu\text{mol}/\text{m}^2/\text{s}$ supplemented with kanamycin (50 mg/L), hygromycin (50 mg/L) or phosphinothricin (6 mg/L, for Bar resistance), and genotyped by PCR. T1 heterozygous and T2 or T3 homozygous *CBM11-IBP/BIBPΔ* *Arabidopsis* plants were selected and analysed with kanamycin and hygromycin and PCR genotyping. *CBM11-IBP-Dendra2* *Arabidopsis* plants were selected with phosphinothricin and BASTA spray. Rice was transformed with *CBM11-IBP* and *CBM11-Roo* using Agrobacterium-mediated method described previously (Nishimura *et al.*, 2006). Briefly, seeds from *O. sativa* var. *japonica* 'Nipponbare' were surface-sterilized and germinated on N6 medium [Chu's N6 medium with vitamins supplemented with 2 mg/L 2,4-dichlorophenoxyacetic acid (2,4-D), 0.1 g myo-inositol, 0.3 g/L casein hydrolysate, 2.878 g L-proline and 3% sucrose, pH, 5.8, solidified with 4 g phytigel] to initiate calli. After incubation for 3–4 weeks at 30 °C, light (110 $\mu\text{mol}/\text{m}^2/\text{s}$), actively growing calli (yellowish white) were collected and proliferated on the same medium to be used for Agrobacterium cocultivation (3 days, at 28 °C in dark). Infected calli were washed with sterile water and selected with N6 medium with 50 mg/L hygromycin and 250 mg/L carbenicillin for 3–4 weeks at 30 °C, light at 110 $\mu\text{mol}/\text{m}^2/\text{s}$. Hygromycin-resistant calli were transferred to rice shoot regeneration medium (4.4 g/L MS salts, 2.0 mg/L 6-benzylaminopurine, 30 g/L sucrose, 7 g/L TC agar), and regenerated shoots were transferred to

full-strength MS medium with 2% sucrose and 0.7% agar. Twenty transgenic lines for *Arabidopsis* and more than ten lines for rice were generated. Three lines were continued to homozygosity for detailed analyses. T3 homozygous transgenic plants were selected with hygromycin (50 mg/L) and confirmed by PCR genotyping.

Plant growth conditions

Arabidopsis wild-type and *CBM11-FIBP/CBM-IBP* seedlings were grown as above except as indicated for specific treatments. *Arabidopsis* wild-type and *CBM11-FIBP/CBM-IBP* plants were grown in the greenhouse in soil under natural light conditions, except the day length was extended to 16 h with HID lights (150 $\mu\text{mol/m}^2/\text{s}$) in the winter. See www.hort.purdue.edu/hort/facilities/greenhouse/hlaTech.shtml for more information. Plants were watered with 1/10 strength Hoagland's nutrient solution (Barac *et al.*, 2004) supplemented with 100 μm iron every 2 weeks or with 1/10 strength Hoagland's nutrient solution supplemented with a 0.5 mm iron solution (Sequestrene 330 Fe, Becker Underwood, INC, Ames, IA) foliar spray once every 2 weeks (3 times in total). The floral spray was developed as a more environmentally friendly iron application method for biofuel feedstock production. Rice wild-type and *CBM-IBP* seedlings were grown on 0.45% phytigel plates, containing quarter-strength MS, pH 5.5, 22 °C, 14 h light (100 $\mu\text{mol/m}^2/\text{s}$) except as indicated for specific treatments. Rice wild-type and *CBM-IBP* plants were grown in the greenhouse in calcined clay (Profile Greens calcined clay granules in 9-cm pots) with drip irrigation under semi-dry and natural light conditions, and in the winter, the day length was extended to 16 h with HID lights (250 $\mu\text{mol/m}^2/\text{s}$). The rice plants were watered and fertilized with 1/10 Hoagland's solution supplemented with 50 μm iron or 1/10 Hoagland's solution supplemented with a 0.5 mm iron foliar spray every 2 weeks after flowering (three applications in total). Before harvest, tiller numbers were counted and plant heights were measured from the root-shoot junction to the tip of the tallest flag leaf. Plant biomass and seeds were harvested and dried in a laminar flow hood at room temperature for 1 week, and dry weights were recorded. The *CBM-IBP* *Arabidopsis* and rice plants contained similar amounts of iron in both soil and foliar Fe application, so the iron concentration was independent of the fertilization method.

Quantitative RT-PCR analysis of transgenic *Arabidopsis* and rice

Total RNA was isolated from 7-days *Arabidopsis* or 10-days rice seedlings using the RNeasy Mini Kit according to the vendor's manual (Qiagen, www.qiagen.com). RNA was quantified and treated with TURBO DNA-freeTM DNase (Ambion RNA by Life Technologies, www.invitrogen.com). First-strand cDNA was synthesized from three μg of total RNA with the SuperScript[®] III reverse transcription kit followed by reverse transcription, according to the vendor's manual (Invitrogen). Quantitative RT-PCR was performed using the CFX96 real-time PCR detection system (Bio-Rad, www.Bio-Rad.com) and GoTaq[®] qPCR Master Mix (Promega, www.promega.com). See Table S2 for the primers.

Iron staining

Arabidopsis and rice seedlings were vacuum-infiltrated with Perls' Prussian blue stain solution (equal volumes of 4% [v/v] HCl and 4% [w/v] K-ferrocyanide) for 15 min. The plant samples were incubated for 30 min, rinsed three times with water and stored in

70% ethanol. The staining was imaged using a Zeiss Observer Z1 microscope (Carl Zeiss, Jena, Germany). Stained samples were imbedded in Neg-50 frozen section medium (Richard-Allan Scientific, Kalamazoo, MI). 100- μm -thick sections were prepared in Microm HM550 (Microm International GmbH, Walldorf, Germany) and imaged using a Zeiss Observer Z1 microscope (Carl Zeiss, Jena, Germany).

Immunohistochemical localization, immunofluorescence and fluorescent protein localization studies

Arabidopsis 5-d seedlings were prepared for immunolocalization as described in Peer *et al.* (Peer *et al.*, 2009) Briefly, seedlings were fixed in 4% *p*-formaldehyde in microtubule-stabilizing buffer (MTSB) solution (50 mM PIPES, 5 mM EGTA, and 5 mM MgSO₄) and 5% DMSO for 1 h. They were washed with MTSB + 0.1% Nonidet P-40 for 10 min (five times). The seedlings were permeabilized for 1 h in 10% DMSO and 1% Nonidet P-40 and then blocked with 3% BSA in MTSB for 3 h. The seedlings were incubated overnight (37 °C) with anti-HA (1 : 250, Santa Cruz Biotechnology, www.scbt.com), in 3% BSA in MTSB. They were then washed for 10 min (six times) in 0.1% Triton X-100, for 10 min (three times) in MTSB, and then incubated for 3 h at 37 °C in goat anti-rabbit-Alexa Fluor 488 (1 : 250) in 3% BSA/MTSB. The seedlings were washed in MTSB/0.1% Triton X-100 and then in water for 10 min each (five times). Immunofluorescence analysis was performed using a Zeiss LSM 710 confocal laser scanning microscope (Carl Zeiss, Jena, Germany). The following settings were used: for Alexa Fluor 488: 488 nm argon laser at 3.5%, pinhole 90 μm , emission 493–630 nm, gain 650, pixel dwell 6.3 μs ; for YFP: 514 nm argon laser at 13%, pinhole 90 μm , emission 519–621 nm, gain 833, pixel dwell time 3.15 μs ; and for mCherry: 543 nm argon laser at 60%, pinhole 45 μm , emission 578–696 nm, gain 821, pixel dwell time 6.3 μs . The oestrogen-inducible *CBM-IBP-Dendra2* *Arabidopsis* plants were germinated on $\frac{1}{4}$ strength MS plates. Three-day-old seedlings were transferred to plates with $\frac{1}{4}$ strength MS containing 4 μm 4-hydroxy tamoxifen for 16–40 h. *CBM-IBP-Dendra2* signals were analysed using 488 nm argon laser at 24%, pinhole 90 μm , emission 493–577 nm, gain 820, pixel dwell 3.15 μs .

X-ray fluorescence microscopy

Four-week-old bolted *Arabidopsis* plants were sprayed with iron solution (0.5 mm) once. Inflorescence stems were dissected and imbedded in 5% agar when cooled to ~50 °C. 100- μm -thick sections were prepared using a TPI Vibratome 1000. Sections were sent to Argonne National Laboratory for analysis according to method described in Inouye *et al.* (2014).

Elemental analyses

Arabidopsis and rice shoot tissues were harvested when fully senescent, air-dried and shaken to remove the seeds. Dry *Arabidopsis* and rice shoots were ground twice to pass through a 20-mesh (1-mm) screen using a Wiley Mill. The husk was removed from dry rice seeds to obtain brown rice; brown rice was polished to white rice according to Wirth *et al.* (2009). Both brown and white rice grains were ground into a fine powder using a mortar and pestle. An aliquot of the ground samples was used to measure the metal concentrations with modifications to published procedures (Stacey *et al.*, 2008; Vansuyt *et al.*, 2007; Wei and Layzell, 2006). Briefly, 20 mg of dry, ground sample was digested in 0.4 mL 25% (v/v) nitric acid (Trace Metal Grade,

Fisher Scientific), at 70 °C, overnight. After digestion, the extract was diluted to 5 mL with fresh Millipore (Synergy Water Purification System) de-ionized H₂O (the final nitric acid concentration was 2%) and analysed quantitatively for iron and other metal ions using inductively coupled plasma-optical emission spectroscopy (ICP-OES) by the Chemical Analysis Laboratory at the University of Georgia. Trial experiments indicated that the recovery rates for the ions during the nitric acid extractions were between 97% and 102%; thus, the original data have been presented without adjustments.

Biomass pretreatment and conversion to sugars

Arabidopsis and rice shoot tissues were harvested when fully senescent, air-dried and shaken to remove the seeds, ground twice to pass through a 20-mesh (1-mm) screen using a Wiley Mill and then tested for total sugar release through hot water pretreatment combined with enzymatic hydrolysis, using a high-throughput (HTP) type pretreatment procedure is that it can process large numbers of biomass samples with small sample sizes to test sugar release (Decker *et al.*, 2009; Selig *et al.*, 2010; Studer *et al.*, 2010, 2011). Briefly, 5 mg of ground biomass from each plant line was weighed manually in sample replicates into individual wells on 96-well Hastelloy plates; water was added, the plates sealed, clamped and subjected to hot water pretreatment and cosaccharification, using a high-throughput analytical process developed by NREL. The hot water pretreatment was conducted at 180 °C for 17.5 min. Following hot water pretreatment, the seals were pierced with a 96-point punch to allow the addition of buffer and enzymes. The pH of pretreated biomass slurry was buffered at pH 5.0 by addition of 1 M sodium citrate buffer containing the desired enzymes (as described below) to ensure an optimal condition for enzymatic saccharification. A total volume of 40 µL of buffer and enzyme was added to each well; the enzyme used was Novozymes CTec2 (3 mg enzyme/g biomass). The 96-well plate was resealed, and the enzymatic cosaccharification was carried out at 40 °C for 70 h. After the cosaccharification, the sugar release was analysed using glucose oxidase/peroxidase (GOPOD) assay for glucose and xylose dehydrogenase (XDH) assay for xylose as described previously (Gao *et al.*, 2013; Selig *et al.*, 2010).

Rice grain size analyses

100-grain rice seeds were collected from each plant and dry weights determined on a balance. Scanned pictures of collected rice grains were analysed using SmartGrain software program (Tanabata *et al.*, 2012).

Cellulose and sugar quantifications

Arabidopsis and rice shoot tissues were harvested when fully senescent, air-dried and shaken to remove the seeds, ground twice to pass through a 20-mesh (1-mm) screen using a Wiley Mill. To determine cellulose concentration of rice straw and Arabidopsis shoot biomass, 15 mg samples were weighed into conical glass centrifuge tubes with screw caps, three biological replicates each. After adding 3 mL of a mixture of acetic acid/water/nitric acid (8/2/1, v/v/v), the suspension was incubated at 100 °C for 90 min with occasional mixing (Updegraff, 1969). After cooling, the tubes were centrifuged at 2500 g for 3 min and the supernatant discarded. The pellet was washed three times with water, centrifuged at 2500 g for 3 min and water discarded each time. The pellet was resuspended in 3 mL water

and 250 µL was taken for phenol-sulphuric assay (Dubois *et al.*, 1956); 250 µL of 5% phenol was added to each tube and mixed; and 2.5 mL of H₂SO₄ was added and vortexed to mix. Samples were incubated overnight at ambient temperature and read at 500 nm compared to cellulose standards (Sigmacell; Sigma).

To remove soluble sugars, 0.5 g dry biomass was incubated with 10 mL 50% ethanol at 70 °C for 20 min. The supernatant was dried under evaporator and sugar content was determined by phenol-sulphuric acid assay (Dubois *et al.*, 1956). The pellet was washed once with 50% ethanol and five times with water. Alcohol-insoluble residues were freeze-dried and used for neutral sugar analysis.

Neutral sugar composition was analysed according to Gibeaut and Carpita (1991). Briefly, wall material (alcohol-insoluble residues) was hydrolysed in 2 N trifluoroacetic acid (TFA) containing 0.5 µmol of myo-inositol (internal standard) for 90 min at 120 °C. The TFA was evaporated in a stream of N₂. Sugars were dissolved in 100 µL of 1 M NH₄OH and 0.5 mL of 20 mg/mL NaBH₄ in DMSO (w/v) and incubated at 45 °C for 90 min with occasional vortex mixing. The solution was neutralized with 100 µL of glacial acetic acid, and then, 100 µL of 1-methylimidazole (Sigma) followed by 0.75 mL of acetic anhydride was added, and the mixture was incubated at 42 °C for 30 min. Water (1.5 mL) was added to destroy unreacted acetic anhydride, and when cool, the alditol acetates were partitioned into CH₂Cl₂. The entire reaction was completed in 1-dram vials sealed with Teflon-lined caps. Derivatives were separated by gas-liquid chromatography (GLC) on a 0.25 mm × 30 m column of SP-2330 (Supelco, Bellefonte, PA). Temperature was held at 80°C during injection, then ramped to 170 °C at 25 °C/min and then to 240 °C at 5 °C/min, with a 10-min hold at the upper temperature. Helium flow was 1 mL/min with split-less injection. The electron impact mass spectrometry (EIMS) was performed with a Hewlett-Packard MSD at 70 eV and a source temperature of 250 °C.

Antigenicity analyses

Antigen analyses were conducted using the precision tool at the Immunomedicine Group at University of Madrid (<http://imed.mecd.ucm.es/Tools/antigenic.pl>). The synthetic iron-binding peptidase based on the blood iron-binding sequence DLGEQYFKG (Lee and Song, 2009), CtCBM11_2LRP_A from the crystal structure and rice alpha-expansin AAL24493.1. The prediction tool is based on the algorithms in Kolaskar and Tongaonkar (1990).

Acknowledgements

This work was supported by the Center for Direct Catalytic Conversion of Biomass to Biofuels (C³Bio), an Energy Frontier Research Center funded by the U.S. Department of Energy, Office of Science, Office of Basic Energy Sciences (Award Number DE-SC0000997). We thank Steve Decker, Crissa Doeppke, Erica Gjersing, Geoffrey Turner and Angela Ziebell of NREL HPT team for HTP hot pretreatment and cosaccharification analysis of plant biomass. Use of the Advanced Photon Source, an Office of Science User Facility operated for the U.S. Department of Energy (DOE) Office of Science by Argonne National Laboratory, was supported by the U.S. DOE under Contract No. DE-AC02-06CH11357. We declare no conflict of interest. Support for the contribution from ASM was provided by the US Department of Energy, Chemical Sciences, Geosciences, & Biosciences DE-FG02-06ER1580.

References

- Alder, A., Jamil, M., Bruno, M., Vermathen, M., Bigler, P., Ghisla, S., Bouwmeester, H. et al. (2012) The path from β-carotene to carlactone, a strigolactone-like plant hormone. *Science*, **335**, 1348–1351.
- Baldwin, K., Childs, N., Dyck, J. and Hansen, J. (2012) *A Report from the Economic Research Service Southeast Asia's Rice Surplus*. RCS-12 I-01 Economic Research Service/USDA. Available at: <http://www.ers.usda.gov/media/978994/rccs-12l-01.pdf>
- Barac, T., Taghavi, S., Borremans, B., Provoost, A., Oeyen, L., Colpaert, J.V., Vangronsveld, J. et al. (2004) Engineered endophytic bacteria improve phytoremediation of water-soluble, volatile, organic pollutants. *Nat. Biotechnol.* **22**, 583–588.
- Beckham, G.T., Dai, Z., Matthews, J.F., Momany, M., Payne, C.M., Adney, W.S., Baker, S.E. et al. (2012) Harnessing glycosylation to improve cellulase activity. *Curr. Opin. Biotechnol.* **23**, 338–345.
- Boraston, A.B., Bolam, D.N., Gilbert, H.J. and Davies, G.J. (2004) Carbohydrate-binding modules: fine-tuning polysaccharide recognition. *Biochem. J.* **382**, 769–781.
- Brooks, B.R., Brooks, C.L., Mackerell, A.D., Nilsson, L., Petrella, R.J., Roux, B. and Won, Y. et al. (2009) CHARMM: the biomolecular simulation program. *J. Comput. Chem.* **30**, 1545–1614.
- Chereskin, B.M. and Castelfranco, P.A. (1982) Effects of iron and oxygen on chlorophyll biosynthesis: II. Observations on the biosynthetic pathway in isolated etioplasts. *Plant Physiol.* **69**, 112–116.
- Cho, H.T. and Cosgrove, D.J. (2000) Altered expression of expansin modulates leaf growth and pedicel abscission in *Arabidopsis thaliana*. *Proc. Natl. Acad. Sci. USA*, **97**, 9783–9788.
- Choi, D., Lee, Y., Cho, H.-T. and Kende, H. (2003) Regulation of expansin gene expression affects growth and development in transgenic rice plants. *Plant Cell*, **15**, 1386–1398.
- Clough, S.J. and Bent, A.F. (1998) Floral dip: a simplified method for Agrobacterium-mediated transformation of *Arabidopsis thaliana*. *Plant J.* **16**, 735–743.
- De Loose, M., Gheysen, G., Tiré, C., Gielen, J., Villarroel, R., Genetello, C., Van Montagu, M. et al. (1991) The extensin signal peptide allows secretion of a heterologous protein from protoplasts. *Gene*, **99**, 95–100.
- Decker, S.R., Brunecky, R., Tucker, M.P., Himmel, M.E. and Selig, M.J. (2009) High-throughput screening techniques for biomass conversion. *Bioenergy Res.* **2**, 179–192.
- Dubois, M., Gilles, K.A., Ton, J.K.H., Rebers, P.A. and Smith, F. (1956) Colorimetric method for determination of sugars and related substances. *Anal. Chem.*, **28**, 350–356.
- Fang, H.-M. and Wang, Y. (2002) Characterization of iron-binding motifs in *Candida albicans* high-affinity iron permease CaFtr1p by site-directed mutagenesis. *Biochem. J.* **368**, 641–647.
- Gao, Y., Xu, J., Zhang, Y., Yu, Q., Yuan, Z. and Liu, Y. (2013) Effects of different pretreatment methods on chemical composition of sugarcane bagasse and enzymatic hydrolysis. *Bioresour. Technol.* **144**, 396–400.
- Gibeaut, D.M. and Carpita, N.C. (1991) Tracing the biosynthesis of the cell wall in intact cells and plants. Selective turnover and alteration of cytoplasmic and cell wall polysaccharides of proso millet cells in liquid culture and Zea mays seedlings. *Plant Physiol.* **97**, 551–561.
- Goto, F., Yoshihara, T., Shigemoto, N., Toki, S. and Takaiwa, F. (1999) Iron fortification of rice seed by the soybean ferritin gene. *Nat. Biotechnol.* **17**, 282–286.
- Guvench, O., Greene, S.N., Kamath, G., Brady, J.W., Venable, R.M., Pastor, R.W. and Mackerell, A.D. (2008) Additive empirical force field for hexopyranose monosaccharides. *J. Comput. Chem.* **29**, 2543–2564.
- Guvench, O., Hatcher, E., Venable, R.M., Pastor, R.W. and MacKerell, A.D. (2009) CHARMM additive all-atom force field for glycosidic linkages between hexopyranoses. *J. Chem. Theory Comput.* **5**, 2353–2370.
- Hall, Q. and Cannon, M.C. (2002) The cell wall hydroxyproline-rich glycoprotein RSH is essential for normal embryo development in *Arabidopsis*. *Plant Cell*, **14**, 1161–1172.
- Harris, D.C. (1998) *Quantitative Chemical Analysis*, 5th edn. Freeman and Company, New York, NY. p. 804.
- Hashimoto, H. (2006) Recent structural studies of carbohydrate-binding modules. *Cell. Mol. Life Sci.* **63**, 2954–2967.
- Hill, J., Nelson, E., Tilman, D., Polasky, S. and Tiffany, D. (2006) Environmental, economic, and energetic costs and benefits of biodiesel and ethanol biofuels. *Proc. Natl. Acad. Sci. USA*, **103**, 11206–11210.
- Himmel, M.E., Ding, S.-Y., Johnson, D.K., Adney, W.S., Nimlos, M.R., Brady, J.W. and Foust, T.D. (2007) Biomass recalcitrance: engineering plants and enzymes for biofuels production. *Science*, **315**, 804–807.
- Inouye, H., Zhang, Y., Yang, L., Venugopalan, N., Fischetti, R.F., Gleber, S.C., Vogt, S. et al. (2014) Multiscale deconstruction of molecular architecture in corn stover. *Sci. Rep.* **4**, 3756.
- Jásik, J., Boggetti, B., Baluška, F., Volkmann, D., Gensch, T., Rutten, T., Altmann, T. et al. (2013) PIN2 turnover in *Arabidopsis* root epidermal cells explored by the photoconvertible protein Dendra2. *PLoS ONE*, **8**, e61403.
- Kamireddy, S.R., Li, J., Tucker, M., Degenstein, J. and Ji, Y. (2013) Effects and mechanism of metal chloride salts on pretreatment and enzymatic digestibility of corn stover. *Ind. Eng. Chem. Res.* **52**, 1775–1782.
- Kolaskar, A.S. and Tongaonkar, P.C. (1990) A semi-empirical method for prediction of antigenic determinants on protein antigens. *FEBS Lett.* **276**, 172–174.
- Lamport, D.T.A., Kieliszewski, M.J., Chen, Y. and Cannon, M.C. (2011) Role of the extensin superfamily in primary cell wall architecture. *Plant Physiol.* **156**, 11–19.
- Lawson, D.M., Artyukh, P.J., Yewdall, S.J. et al. (1991) Solving the structure of human H ferritin by genetically engineering intermolecular crystal contacts. *Nature*, **349**, 541–544.
- Lee, S.-H. and Song, K.B. (2009) Purification of an iron-binding nonapeptide from hydrolysates of porcine blood plasma protein. *Process Biochem.* **44**, 378–381.
- Lin, H., Wang Qian, R.Q., Yan, M., Meng, X., Fu, Z., Yan, C., Jiang, B. et al. (2009) DWARF27, an iron-containing protein required for the biosynthesis of strigolactones, regulates rice tiller bud outgrowth. *Plant Cell*, **21**, 1512–1525.
- Liu, L., Sun, J., Cai, C., Wang, S., Pei, H. and Zhang, J. (2009) Corn stover pretreatment by inorganic salts and its effects on hemicellulose and cellulose degradation. *Bioresour. Technol.* **100**, 5865–5871.
- MacKerell, A.D., Bashford, D., Bellott, M. et al. (1998) All-atom empirical potential for molecular modeling and dynamics studies of proteins. *J. Phys. Chem. B*, **102**, 3586–3616.
- Meng, F., Wei, Y. and Yang, X. (2005) Iron content and bioavailability in rice. *J. Trace Elem. Med. Biol.* **18**, 333–338.
- Nakagawa, T., Kurose, T., Hino, T., Tanaka, K., Kawamukai, M., Niwa, Y., Toyooka, K. et al. (2007) Development of series of gateway binary vectors, pGWBs, for realizing efficient construction of fusion genes for plant transformation. *J. Biosci. Bioeng.* **104**, 34–41.
- Nishimura, A., Aichi, I. and Matsuoka, M. (2006) A protocol for Agrobacterium-mediated transformation in rice. *Nat. Protoc.* **1**, 2796–2802.
- Palmer, C.M. and Guerinet, M.L. (2009) Facing the challenges of Cu, Fe and Zn homeostasis in plants. *Nat. Chem. Biol.* **5**, 333–340.
- Payne, C.M., Himmel, M.E., Crowley, M.F. and Beckham, G.T. (2011) Decrystallization of oligosaccharides from the cellulose I β surface with molecular simulation. *J. Phys. Chem. Lett.* **2**, 1546–1550.
- Peer, W.A., Hosein, F.N., Bandyopadhyay, A., Makam, S.N., Otegui, M.S., Lee, G.J., Blakeslee, J.J. et al. (2009) Mutation of the membrane-associated M1 protease APM1 results in distinct embryonic and seedling developmental defects in *Arabidopsis*. *Plant Cell*, **21**, 1693–1721.
- Qu, Q.L., Yoshihara, T., Ooyama, A., Goto, F. and Takaiwa, F. (2005) Iron accumulation does not parallel the high expression level of ferritin in transgenic rice seeds. *Planta*, **222**, 225–233.
- Selig, M.J., Tucker, M.P., Sykes, R.W., Reichel, K.L., Brunecky, R., Himmel, M.E., Davis, M.F. et al. (2010) Original Research: Lignocellulose recalcitrance screening by integrated high-throughput hydrothermal pretreatment and enzymatic saccharification. *Ind. Biotechnol.* **6**, 104–111.
- Shaner, N.C., Steinbach, P.A. and Tsien, R.Y. (2005) A guide to choosing fluorescent proteins. *Nat. Methods*, **2**, 905–909.
- Shoseyov, O., Shani, Z. and Levy, I. (2006) Carbohydrate binding modules: biochemical properties and novel applications. *Microbiol. Mol. Biol. Rev.* **70**, 283–295.
- Stacey, M.G., Patel, A., McClain, W.E., Mathieu, M., Remley, M., Rogers, E.E., Gassmann, W. et al. (2008) The *Arabidopsis* AtOPT3 protein functions in

- metal homeostasis and movement of iron to developing seeds. *Plant Physiol.* **146**, 589–601.
- Studer, M.H., DeMartini, J.D., Brethauer, S., McKenzie, H.L. and Wyman, C.E. (2010) Engineering of a high-throughput screening system to identify cellulosic biomass, pretreatments, and enzyme formulations that enhance sugar release. *Biotechnol. Bioeng.* **105**, 231–238.
- Studer, M.H., DeMartini, J.D., Davis, M.F., Sykes, R.W., Davison, B., Keller, M., Tuskan, G.A. *et al.* (2011) Lignin content in natural *Populus* variants affects sugar release. *Proc. Natl. Acad. Sci. USA*, **108**, 6300–6305.
- Tanabata, T., Shibaya, T., Hori, K., Ebana, K. and Yano, M. (2012) SmartGrain: high-throughput phenotyping software for measuring seed shape through image analysis. *Plant Physiol.* **160**, 1871–1880.
- Updegraff, D.M. (1969) Semimicro determination of cellulose in biological materials. *Anal. Biochem.* **32**, 420–424.
- Vansuyt, G., Robin, A., Briat, J.-F., Curie, C. and Lemanceau, P. (2007) Iron acquisition from Fe-pyroverdine by *Arabidopsis thaliana*. *Mol. Plant Microbe Interact.* **20**, 441–447.
- Viegas, A., Sardinha, J., Freire, F., Duarte, D.F., Carvalho, A.L., Fontes, C.M.G.A., Romão, M.J. *et al.* (2013) Solution structure, dynamics and binding studies of a family 11 carbohydrate-binding module from *Clostridium thermocellum* (CtCBM11). *Biochem. J.* **451**, 289–300.
- Wei, H. and Layzell, D.B. (2006) Adenylate-coupled ion movement. A mechanism for the control of nodule permeability to O₂ diffusion. *Plant Physiol.* **141**, 280–287.
- Wei, H., Donohoe, B.S., Vinzant, T.B., Ciesielski, P.N., Wang, W., Gedvilas, L.M., Zeng, Y. *et al.* (2011) Elucidating the role of ferrous ion cocatalyst in enhancing dilute acid pretreatment of lignocellulosic biomass. *Biotechnol. Biofuels*, **4**, 48.
- Wirth, J., Poletti, S., Aeschlimann, B., Yakandawala, N., Drosse, B., Osorio, S., Tohge, T. *et al.* (2009) Rice endosperm iron biofortification by targeted and synergistic action of nicotianamine synthase and ferritin. *Plant Biotechnol. J.* **7**, 631–644.
- Wu, M., Bu, L., Vuong, T.V., Wilson, D.B., Crowley, M.F., Sandgren, M., Ståhlberg, J. *et al.* (2013) Loop motions important to product expulsion in the *Thermobifida fusca* glycoside hydrolase family 6 cellobiohydrolase from structural and computational studies. *J. Biol. Chem.* **288**, 33107–33117.
- Zeng, Y., Zhang, H., Wang, L., Pu, X., Du, J., Yang, S. and Liu, J. (2010) Genotypic variation in element concentrations in brown rice from Yunnan landraces in China. *Environ. Geochem. Health*, **3**, 165–177.
- Zeng, Y., Zhang, H., Wang, L., Pu, X., Du, J., Yang, S. and Liu, J. (2010) Genotypic variation in element concentrations in brown rice from Yunnan landraces in China. *Environ. Geochem. Health* **32**, 165–177.
- Zhao, J., Zhang, H., Zheng, R., Lin, Z. and Huang, H. (2011) The enhancement of pretreatment and enzymatic hydrolysis of corn stover by FeSO₄ pretreatment. *Biochem. Eng. J.* **56**, 158–164.

Supporting information

Additional Supporting information may be found in the online version of this article:

Figure S1 Expression of *CBM-mCherry* and *CBM-IBP* in *Arabidopsis*.

Figure S2 Cellulose and sugar analysis of Col-0, *CBM-IBP* and *CBM-IBPΔ* biomass.

Figure S3 Characterization of *CBM-IBP* rice plants: expression levels, plant height, chlorophyll concentration, and cellulose and sugar composition.

Figure S4 Characterization of wild type (WT) and *CBM-IBP* rice grains.

Table S1 Seed element profile of *CBM-IBP* and control *Arabidopsis* and rice plants (μg/g dry weight).

Table S2 Primer list.